MODELLING LOW VELOCITY IMPACT IN C/EPOXY LAMINATES

E. Arévalo[1], C. González,[1], F. Gálvez[1] y J. LLorca[1]

[1]Department of Material Science. Polytechnic University of Madrid. ETS de Ingenieros de Caminos. c/Profesor Aranguren s/n. Madrid 28040. Spain

The development of accurate damage models to predict the energy absorption in C/epoxy laminates is an area of increasing interest in composite engineering. Virtual tests of low velocity impact were performed using the finite element explicit code ABAQUS including the experimental damage mechanisms experimentally observed. A constitutive 3D continuum damage mechanics model was implemented in the code as a VUMAT user material subroutine and standard cohesive elements were inserted at the interface between composite plies to simulate delamination damage. Force versus time histories and absorbed energy were compared with experimental results on C/epoxy laminates and showed good agreement.

INTRODUCTION

Carbon fiber reinforced polymers materials are extensively used in applications where weight saving without decreasing performance and reliability is needed. The main drawback of these materials is the limited damage tolerance as compared with standard metallic alloys especially during impact events such as bird strikes against aeronautical structures. The classic empirical approach to design an optimum composite structure that increases the energy absorption and supports higher impact loads always involve numerous and costly tests. Moreover, certification of safety requires carrying out tests on material coupons, subcomponents and the whole structural elements. At this point, finite element computational models emerged as accurate tools to investigate the mechanical behaviour of structural materials due to their ability to include complex constitutive equations and to the increasing power of digital computers [1,2,3]. This methodology which simulates the mechanical behaviour of simple composite structures until fracture is applied in this paper to study the low speed impact induced by a drop weight impactor on a C/epoxy laminate. The main damage mechanisms experimentally observed were explicitly taken into account in the model as intralaminar damage –using a constitutive equation derived from the continuum damage mechanics framework- and interlaminar damage using interface elements.

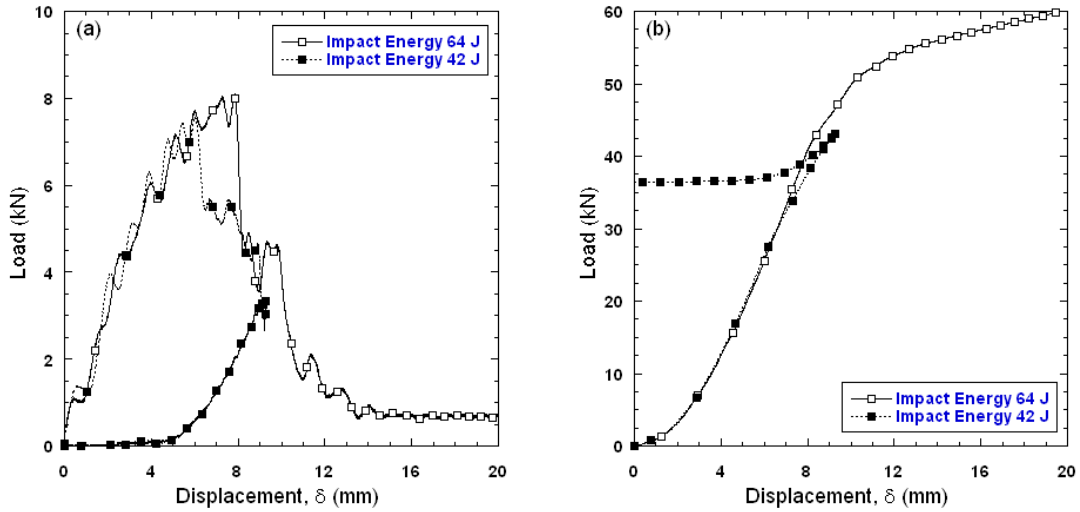

Figure 1. Experimental load-displacement (a) and absorbed energy (b) of the 4.4 mm $[(45/0)_3]_s$ specimen impacted with 64 and 42 J. They stand for tests with and without penetration, respectively.

MATERIALS AND EXPERIMENTAL RESULTS

Materials and experimental techniques

Composite panels were produced by Airbus Spain using the resin transfer moulding technique. A carbon woven preform (G0926 5HS) was infiltrated with a standard RTM6 epoxy resin. The composite panels were consolidated and cured in vacuum at 180°C for 2 hours. The stacking sequences were $[(45/0)_3]_S$, $[(45/0)_4]_S$, $[(45/0)_5]_S$ corresponding to panel thicknesses of t=4.4, 5.9 and 7.4 mm, respectively.

Square specimens of 145x145 mm^2 were cut from the composite panels. Low velocity impact tests were carried out using a DynaTup 8250 drop weight testing machine. The composite plates were simply supported to the fixture at the edges with special clamping tweezers and free impact area of 127x127 mm^2. The specimens were impacted at the center using a 1/2 inch diameter steel tup. Incident impact energies in the range 24 to 209 J to obtain fully penetrated and no penetrated specimens were chosen. The impactor was instrumented with an accelerometer to measure and record continuously the applied force, P, the velocity, v, and displacement, δ, of the point where the load is applied. Finally, the failed specimens were cut, Au-Pd sputtered and examined by scanning electron microscopy to ascertain the failure and deformation micromechanisms.

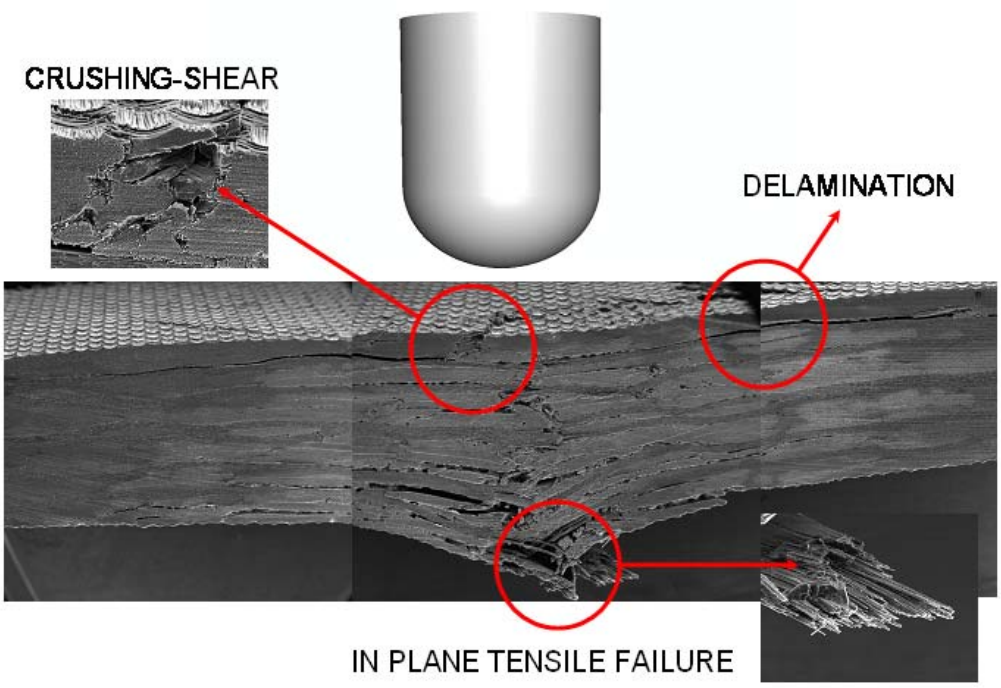

Figure 2. Cross section of a non-penetrated 4.4 mm $[(45/0)_3]_s$ specimen revealing the main damage micromechanisms.

Impact behavior

Four impact tests were carried out for each laminate with a given thickness at room temperature. The impact energies were selected to have two tests with no penetration and two with total or complete penetration. The load-displacement and energy-displacement curves for the material with 4.4 mm in thickness were plotted in Figures 1 (a) and (b) respectively. They showed a very reproducible behavior. The initial response was linear and elastic up to the maximum load instead of local fluctuations due to the propagation of elastic waves. The maximum load was followed by the post peak region in which extensive damage developed around the tup until the specimen was fully penetrated or the impactor bounced (impact energies of 64 and 42 J respectively, Figure 1). One of the non-penetrated specimens was carefully sectioned with a diamond disk and the cross-section was observed using the scanning electron microscopy to reveal the deformation and failure micromechanisms. Severe intralaminar and interlaminar damage were found. Intralaminar damage took place as in-plane tensile failure of the carbon fibers located at back surface where high tensile stresses develop. Moreover,

severe ply damage occurred at the contact surface as compressive through thickness failure and out-of-plane shear failure (Figure 2). Interlaminar cracks running from the impact region towards the plate boundaries were also observed.

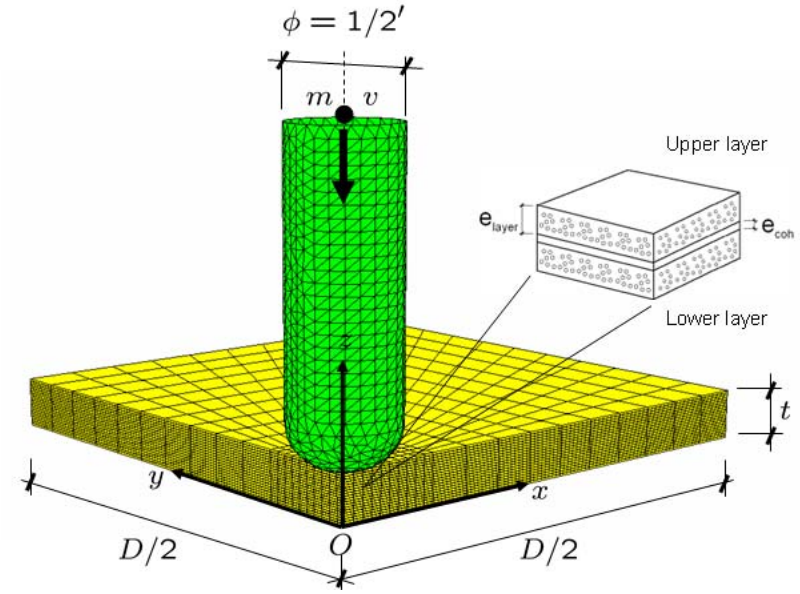

Figure 3. Finite element model of the low velocity impact.

MODELLING

The drop-weight impact tests were modelled by means of finite element method using Abaqus Explicit [4]. The basic strategy used in the simulations is depicted in Figure 3. Due to material and geometry symmetry conditions, only a quarter of the specimen was modelled. Simply supported boundary conditions were applied at those points lying on (x=D/2, y, z=0) and (x, y=D/2, z=0) where D=127 mm is the free distance between supports. Symmetric boundary conditions were applied to all the nodes belonging to OXZ and OYZ cartesian planes. The impactor was modelled as a rigid body (meshed with R3D3 elements in Abaqus) and enforced to move along z with a mass point attached to it. The initial values of the velocity v and the mass point m were selected to represent the appropriate experiments conditions of each simulation.

The main damage mechanisms (intralaminar and interlaminar failure) experimentally observed were included in the simulations. The finite element model explicitly includes the microstructure of the laminate material. Each plate was meshed

using eight node brick elements with reduced integration (C3D8R in Abaqus) with only one element through the thickness per ply. The mechanical behavior of each plate was defined using the Continuum Damage Mechanics framework [5] where the elastic constants of the composite material were degraded progressively as a function of the damage variables. Interlaminar failure was also included in the model by means of eight nodes interface elements (COH3D8 in Abaqus) inserted between two adjacent brick elements representing neighbour plies. The behavior of the interface elements were controlled using a simple cohesive crack model.

Intralaminar failure

The continuum damage mechanics model used to simulate intralaminar failure of the woven fabric layers assumed that the effective behavior of the plate was adequately represented by a linear elastic orthotropic solid. The initial elastic constants of the undamaged material were the elastic moduli E_1,E_2 and E_3, shear moduli G_{12},G_{23} and G_{31} and Poisson's coefficients ν_{12}, ν_{23} and ν_{31} where 1, 2 and 3 denote the local axis of the material in the in-plane fill, warp and out-of-plane directions, respectively, Table (1). This behavior of the material was modified using damage variables (d_i, i=1,6) to include the stiffness degradation due to material damage. The damage variables varied between 0 and 1 for the undamaged and damaged conditions, respectively. The constitutive tensor of the ply as a function of the elastic constants and the damage variables could be expressed as

$$\mathbf{M} = \begin{bmatrix} \frac{1}{(1-d_1)E_1} & -\frac{\upsilon_{12}}{E_1} & -\frac{\upsilon_{13}}{E_1} & 0 & 0 & 0 \\ -\frac{\upsilon_{12}}{E_1} & \frac{1}{(1-d_2)E_2} & -\frac{\upsilon_{23}}{E_2} & 0 & 0 & 0 \\ -\frac{\upsilon_{13}}{E_1} & -\frac{\upsilon_{23}}{E_2} & \frac{1}{(1-d_3)E_3} & 0 & 0 & 0 \\ 0 & 0 & 0 & \frac{1}{(1-d_4)G_{12}} & 0 & 0 \\ 0 & 0 & 0 & 0 & \frac{1}{(1-d_5)G_{13}} & 0 \\ 0 & 0 & 0 & 0 & 0 & \frac{1}{(1-d_6)G_{23}} \end{bmatrix} \quad (1)$$

The state of damage at any material point (i.e. actual values of the damage variables d_i, i=1,6) will remain constant if the stresses (or strains) lie inside of well-defined regions (in analogy to yield surfaces in elasto-plastic materials) expressed mathematically by

ρ (kg/m3)	E_1 (GPa)	E_2 (GPa)	E_3 (GPa)	ν_{12}	ν_{13}	ν_{23}	G_{12} (GPa)	G_{13} (GPa)	G_{23} (GPa)
1500	57.5	57.5	5.75	0.05	0.05	0.05	3.3	3.3	3.3

Table 1. Density and orthotropic elastic constants used in the simulations for the C/epoxy woven lamina (1-2-3 represents fill, warp and out-of-plane directions, respectively.)

$g_j(\varepsilon_{ij}, r_j)$ where j represents a particular damage mechanism. Any point representing the strain tensor of the material must lie either inside ($g_j(\varepsilon_{ij}, r_j) < 0$) the region, or in the boundary of this region $g_j(\varepsilon_{ij}, r_j) = 0$. The set of damage mechanisms observed in the experiments and implemented in the model are: fill and warp fiber tensile/shear failure (2), (3), in-plane compressive failure (4), (5), through thickness compressive failure (6) and in-plane shear matrix failure (7).

$$g_1(\varepsilon_{ij}, r_1) = \left(\frac{E_1\varepsilon_1}{X_T}\right)^2 + \left(\frac{G_{13}\varepsilon_{13}}{S_{13}}\right)^2 - r_1^2 \qquad (2)$$

$$g_2(\varepsilon_{ij}, r_2) = \left(\frac{E_2\varepsilon_2}{Y_T}\right)^2 + \left(\frac{G_{23}\varepsilon_{23}}{S_{23}}\right)^2 - r_2^2 \qquad (3)$$

$$g_3(\varepsilon_{ij}, r_3) = \left(\frac{E_1\varepsilon_1}{X_C}\right)^2 - r_3^2 \qquad (4)$$

$$g_4(\varepsilon_{ij}, r_4) = \left(\frac{E_2\varepsilon_2}{Y_C}\right)^2 - r_4^2 \qquad (5)$$

$$g_5(\varepsilon_{ij}, r_5) = \left(\frac{E_3\varepsilon_3}{Z_C}\right)^2 - r_5^2 \qquad (6)$$

$$g_6(\varepsilon_{ij}, r_6) = \left(\frac{G_{12}\varepsilon_{12}}{S_{12}}\right)^2 - r_6^2 \qquad (7)$$

where r_i, i=1,6 stand for the damage thresholds that dictate the size of evolving damage surface. X_T, X_C, Y_T, and Y_C represent the tensile and compressive strength of the material in the fill and warp directions, and Z_C stands for through thickness or out-of-plane compressive strength, Table 2. Initially, when no damage is present in the material, the thresholds are set to 1 and the equations represent the initial failure criterion for the composite material. The boundaries of the loading surfaces move

outwards with the increasing load and the consistency condition allow to compute the increment of the damage thresholds r_j due to an increase in the strain tensor $\Delta\varepsilon_{ij}$ at a material point. From the consistency condition it can be expressed as

$$\dot{g}_j(\varepsilon_{ij}, r_j, \dot{\varepsilon}_{ij}, \dot{r}_j) = 0 \qquad (8)$$

The evolution of each damage variable d_i should include the coupled effect of several damage mechanisms. According to Matzenmiller *et al*. [5] and Xiao *et. al*. [6], d_i can be computed as

$$d_i = \sum_{j=1}^{6} q_{ij}(1 - e^{\frac{1}{\eta}(1-r_j^{\eta})}) \qquad (9)$$

where q_{ij} is a coefficient matrix which relate the contribution of the damage mechanism j to the damage variable i. Finally η is a strain softening parameter which controls the energy dissipated by damage during the post-peak behaviour of the material. This constitutive equation was programmed in this work as a user subroutine VUMAT in Abaqus Explicit. The strain tensor and the strain increments, ε_{ij} and $\Delta\varepsilon_{ij}$, are introduced in the user subroutine VUMAT at a given time of the simulation, The failure surfaces, equations (2) to (7), are used to compute the updated damage thresholds according to consistency condition (8). The damage thresholds are coupled together according to (9) to obtain the damage variables. With this information, the constitutive equation of the composite is obtained and the stress tensor is updated, equation (1).

X_T/X_T	X_C/X_T	Y_T/X_T	Y_C/X_T	Z_C/X_T	S_{12}/X_T	S_{13}/X_T	S_{23}/X_T	η
1.00	0.275	1.00	0.275	0.827	0.275	0.275	0.275	1/2

Table 2. Relative strength parameters of the composite material used in the simulations (1-2-3 represents fill, warp and out-of-plane directions, respectively.)

Interlaminar failure

Delamination was taken into account in the model by using interface elements inserted between two adjacent layers. In order to speed up computations, the thickness of the interface elements was set to a fraction of the thickness of the adjacent layers representing a resin rich region (typically $e_{coh} = 0.1\ e_{layer}$) between plies, Figure (3). The interface elements transmit stresses according to a cohesive law defined in terms of a traction separation function relating the traction vector applied to the interface element

($\vec{t} = t_n\vec{e}_n + t_s\vec{e}_s + t_t\vec{e}_t$ n, t and s represent the normal and tangential directions of the cohesive elements) and the displacement jump across the interface ($\vec{\delta} =< \delta_n > \vec{e}_n + \delta_s\vec{e}_s + \delta_t\vec{e}_t$) (<> stands for the Macaulay bracket which returns the argument if positive and zero otherwise). A scalar damage parameter D is used again to account for interface degradation. The relations between normal and tangential components of the traction and displacement jump vector can be expressed as

$$t_n = (1-D)K\delta_n \text{ for } \delta_n \geq 0 \text{ and } t_n = K\delta_n \text{ for } \delta_n < 0 \quad (10)$$

$$t_t = (1-D)K\delta_t \quad (11)$$

$$t_s = (1-D)K\delta_s \quad (12)$$

where K represents the elastic stiffness of the interface which was assumed to be the same in all the directions. The interface elements behavior is linear and elastic until the onset of damage. This condition is dictated by the following quadratic interaction criterion

$$(\frac{< t_n >}{N})^2 + (\frac{t_s}{S})^2 + (\frac{t_t}{S})^2 = 1 \quad (13)$$

where N and S represent the interface strength in normal and tangential directions, respectively (assuming isotropic behavior of the interface in tangential plane s-t). Once the strength criterion (13) is fulfilled, the evolution of the damage variable D is controlled by the interface fracture energies in mode I and II (G_I and G_{II}) according to

$$(\frac{G_n}{G_I}) + (\frac{G_s}{G_{II}}) + (\frac{G_t}{G_{II}}) = 1 \quad (14)$$

where G_n, G_s and G_t are the energy spent for each component of the traction vector and its corresponding conjugate relative displacement jump per unit area. The mechanical properties of the interface elements used in the simulations are presented in Table (3). Fully damaged interface elements (D=1) are removed from the model and a contact condition is enforced between the adjacent layers allowing the interaction according to a Coulomb friction criterion with a coefficient μ.

N (MPa)	S (MPa)	G_I (J/m^2)	G_{II} (J/m^2)	μ
33	70	330	800	0.20

Table 3. Mechanical properties of the interface elements used in the simulations.

RESULTS AND DISCUSSION

The load-displacement and energy-displacement curves are plotted in Figure 4 (a) and (b) for the $[(45/0)_3]_S$ and $[(45/0)_5]_S$ specimens and the impact energies of XX and 209 J respectively. The applied load, P, the absorbed energy, E, and the displacement of the load point δ were computed from the acceleration, velocity and displacement of the mass point attached to the impactor. The agreement between simulations and experiments is good in all simulated cases and the maximum load and absorbed energy are adequately captured. The initial slope representing the stiffness of the experimental set-up is also well determined. The results showed also the capability of the methodology to capture the real material failure mechanisms including the penetration or non penetration condition. Delamination damage was also well predicted in the simulations as compared with the damaged areas measured from C-scan images of the failed specimens, Figure 5.

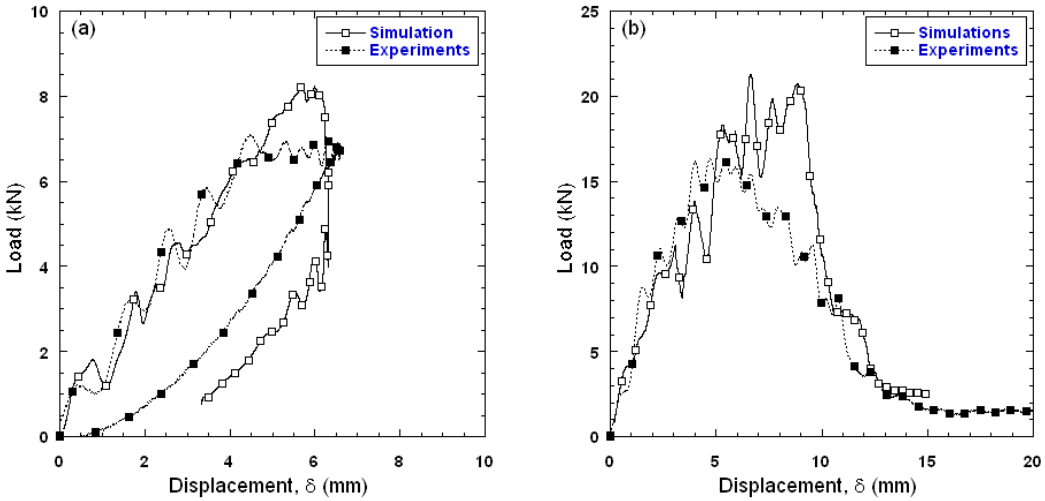

Figure 4. Simulated and experimental load-displacement curves: a) $[(45/0)_3]_S$ specimen and impact energy of 24 J. b) $[(45/0)_5]_S$ specimen and impact energy of 209 J.

ACKNOWLEDGEMENTS

This investigation was supported by Airbus Spain under the project BAITA and by the Ministry of Education and Science through grant MAT2006-02602.

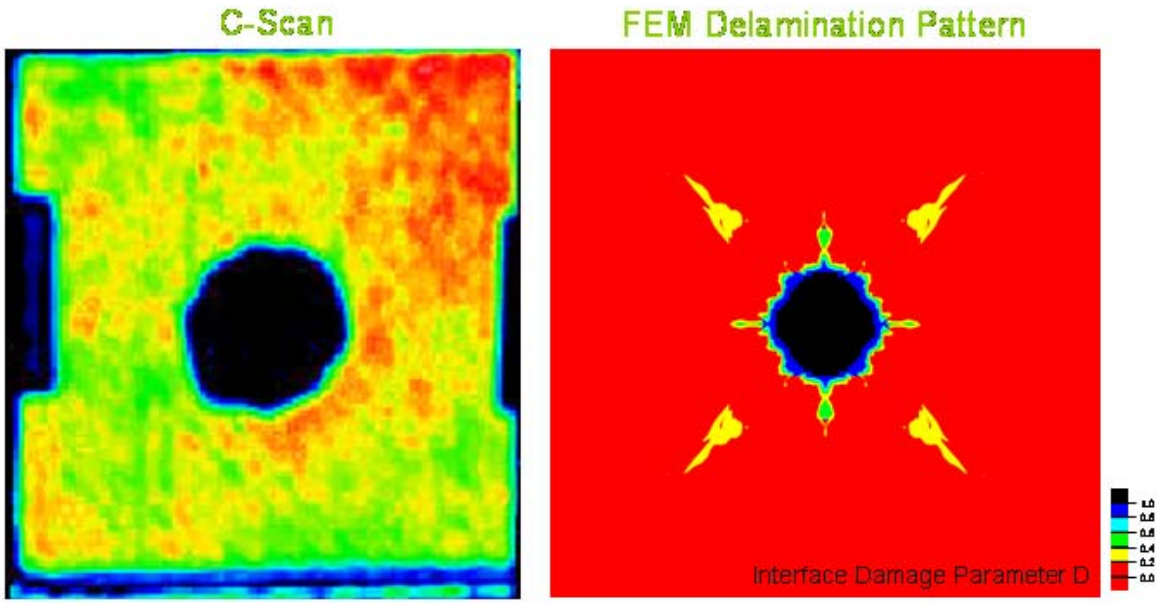

Figure 5. C-scan images and interface damage parameter D of the simulations for the specimen $[(45/0)_5]_S$ and the impact energy of 209 J.

REFERENCES

[1] C. González, J. LLorca, Multiscale modeling of fracture in fiber-reinforced composites, *Acta Materialia*, 54, 4171-4181 (2006)

[2] C. González, J. Segurado, J. LLorca, Numerical simulation of elasto-plastic deformation of composites: Evolution of stress microfields and implications for homogenization models, *Journal of the Mechanics and Physics of Solids*, 52, 1573-1593 (2004)

[3] B. Cox, Q. Yang, In quest of virtual tests for structural composites, *Science*, 314, 1102-1107 (2006)

[4] Abaqus, Users' Manual, ABAQUS, Inc. (2006).

[5] A. Manzenmiller, J. Lubliner, R.L. Taylor, A constitutive model for anisotropic damage in fiber composites, *Mechanics of Materials*, 20, 125-152 (2005)

[6] J.R. Xiao, B.A. Gama, J.W. Gillespie Jr, Progressive damage and delamination in plain weave S-2 glass/SC-15 composites under quasi-static punch-shear loading, *Composite Structures*, 78, 182-196 (2007).